Journal of Power Sources 196 (2011) 5408–5415

Contents lists available at ScienceDirect

Journal of Power Sources

journal homepage: www.elsevier.com/locate/jpowsour

Effect of morphology of mesoporous silica on characterization of protic ionic liquid-based composite membranes

Yun-Sheng Ye[a], Gao-Wei Liang[a], Bo-Han Chen[a], Wei-Chung Shen[a], Chi-Yung Tseng[a], Ming-Yao Cheng[b], John Rick[a], Yao-Jheng Huang[c], Feng-Chih Chang[c], Bing-Joe Hwang[a,*]

[a] Department of Chemical Engineering, National Taiwan University of Science and Technology, Taipei, Taiwan
[b] Graduate Institute of Engineering, National Taiwan University of Science and Technology, Taipei, Taiwan
[c] Institute of Applied Chemistry, National Chiao-Tung University, Hsin-Chu, Taiwan

ARTICLE INFO

Article history:
Received 16 December 2010
Received in revised form 19 February 2011
Accepted 21 February 2011
Available online 26 February 2011

Keywords:
Ionic liquid
Proton exchange membrane
Mesoporous material
Fuel cells
In situ photo crosslinking
Morphology

ABSTRACT

Effects caused by the morphology of mesoporous silica on the characterization of protic ionic liquid-based composite membranes for anhydrous proton exchange membrane applications are investigated. Two types of SBA15 materials with platelet and fiberlike morphologies are synthesized and incorporated into a mixture of polymerizable monomers together with an ionic liquid (IL) [1-butyl-3-methylimidazolium bis(trifluoromethane sulfone)imide (BMIm-TFSI)] to form new conducting membranes using an in situ photo crosslinking process. Incorporation of a defined amount of fiber-shaped SBA 15 and platelet 15 significantly increases the ionic conductivity to between two and three times that of a plain poly(methyl methacrylate) (PMMA)/IL membrane (2.3 mS cm^{-1}) at 160 °C. The protic ionic liquid (PIL) retention ability of the membranes is increased by the capillary forces introduced by the mesoporous silica materials, while ionic conductivity loss after leaching test is retarded. The highest ionic conductivity (5.3 mS cm^{-1}) is obtained by incorporating 5 wt% of P-SBA 15 in the membrane to about six times that of plain PMMA/IL membrane (0.9 mS cm^{-1}) at 160 °C after leaching test.

1. Introduction

One of main issues needing to be addressed with respect to the development of polymer electrolyte membrane fuel cells (PEMFCs) is the development of membrane materials with high operating temperatures (>100 °C), that show: higher reaction kinetics at both electrodes, less poisoning at the anode, and easy heat and water managements of the stacks [1,2]. Nonfluorinated polymeric materials are attracting increasing attention as alternatives to perfluorinated polymer membranes, such as Nafion® or Aciplex-S®, for use as proton exchange membranes (PEMs) in fuel cells; because of their advantages in terms of: cost, monomer toxicity, ease of synthesis, and structural diversity [3,4]. However, these polymers, including Nafion or Aciplex, require humidification to maintain their high proton conductivities, as water molecules play the role of proton carriers; hence, their conductivity is strongly humidity dependent and declines significantly above 100 °C [5].

Protic ionic liquids (PILs) have attracted considerable attention in recent years due to their interesting and potentially useful physicochemical properties, including: high ionic conductivity, high polarity, high density, high heat capacity, and their high thermal and chemical stabilities [6,7]. PILs with these sought after characteristics have been pursued as replacements for liquid electrolytes, which are: toxic, flammable and able to leach out. Recently, fuel cell operation above 100 °C, under anhydrous conditions, has been demonstrated using an anhydrous proton conducting electrolyte. The replacement of water with non-aqueous proton carriers, such as phosphoric acid [8,9] and protic ionic liquids [10–15], has been pursued to obtain PEMs with high conductivities and high thermal stabilities at elevated temperatures under anhydrous conditions. The development of IL-based PEMs focuses mainly on mixtures of well-known polymers with ILs using various strategies, such as: in situ polymerization of vinyl monomers in ILs [10–12], doping polymers with ILs [13], and solution casting IL-polymer solutions [14–16].

Although the IL-based membranes allow PEMFCs to operate at higher temperatures in anhydrous conditions and avoid water dependent conductivity, they have the major drawback of progressively releasing ILs, leading to a long-term decline in the performance of fuel cells [17]. To solve the leaching problem, approaches that incorporate inorganic fillers into the IL-based membranes have been shown to both enhance conductivity and prevent the release of the IL from the composite membranes [10,17]. However, the effect of morphology of mesoporous silica on

* Corresponding author at: Department of Chemical Engineering, National Taiwan University of Science and Technology, #43, Keelung Rd. Sec. 4, Taipei 106, Taiwan. Tel.: +886 2 27376624; fax: +886 2 27376644.
E-mail address: bjh@mail.ntust.edu.tw (B.-J. Hwang).

0378-7753/$ – see front matter © 2011 Elsevier B.V. All rights reserved.
doi:10.1016/j.jpowsour.2011.02.066

characterization of protic ionic liquid-based composite membranes are still not very clear so far.

Mesoporous silica materials have been developed extensively for various applications due to their: high surface areas, narrow pore size distributions, and adjustable mesopore sizes [18–22]. Previous studies of membranes incorporating mesoporous silica spheres have demonstrated significantly improvements in water retention at higher temperatures and a lower relative humidity, together with an enhancement of proton conductivity [18,23,24]. SBA15 has a large surface area and comprises mesoporous silica sieves with long uniform, connecting tubular channels and varying diameter pores (5–50 nm) [21,22,25]. The high surface area should facilitate uniform dispersion in the polymer matrix, thereby yielding more mobile ion species and continuous ion channels to enhance ionic conductivity; however, the diffusion of IL molecules through the lengthy mesochannels and pore blockages are the main concerns when using these materials for IL-based membrane applications. Therefore, the platelet shaped SBA15 with short mesochannels may have significant potential for use in IL-based membranes. In this study, two types of mesoporous silica materials (fiberlike SBA15 and platelet SBA15) were prepared and incorporated into membranes through the in situ photo polymerization of a mixture comprising: polymer precursor (MMA), PIL [1-butyl-3-methylimidazolium bis(trifluoromethane sulfone) imide (BMIm-TFSI)] and mesoporous silica materials. The influence of the morphology, pore size, channel length, as well as the fillers and the IL content on the properties of the resulting composite membranes was systematically investigated with respect to: morphology, ionic conductivity, IL retention properties and thermal stability.

2. Experimental

2.1. Synthesis of 1-butyl-3-methylimidazolium bis(trifluoromethane sulfone)imide (BMIm-TFSI)

The imidazolium tetrafluoroborates with unsaturated aliphatic side chains were prepared according to a modified procedure described elsewhere [11]. In brief, to a stirred solution of 1-methylimidazole (8.91 g, 100 mmol) in acetonitrile (70 mL) was added 1-bromobutane (17.1 g, 110 mmol) 5 in acetonitrile (100 mL) dropwise at 0 °C. The reaction mixture was stirred for 48 h at 30 °C. Removal of the solvent under reduced pressure gave crude 1-butyl-3-methylimidazolium bromide (BMIm-Br), which was recrystallized from petroleum ether. To a solution of the BMIm-Br in acetone (100 mL), was added lithium bis(trifluoromethane sulfone)imide (28.7 g, 100.0 mmol). The resultant viscous oil was washed with deionized water three times, and then dried under vacuum at 80 °C for 24 h before use (yield 85%). The water content was determined as being <0.03 wt% by Karl–Fischer titration.

^{1}H NMR (d6-DMSO): δ 0.88–0.90 (t, $-CH_2-CH_3$), 1.28–1.32 (m, 2H, $-CH_2-CH_2-CH_3$), 1.78–1.81 (m, 2H, $-CH_2-CH_2-CH_2-$), 3.87 (s, 3H, $N-CH_3$), 4.12 (t, 2H, $-N-CH_2-CH_2-$), 7.29–7.31 (s, 1H, –N–CHCH–N–), 8.59 ppm (s, 1H, –N–CH–N–).

2.2. Membrane preparation

A solution comprising different ratios (listed in Table S1) of: methyl methacrylate (MMA), BMIm-TFSI, divinylbenzene (DVB) (5 wt% based on the weight of monomers), benzoln methyl ether (BME), and mesoporous materials was stirred and ultrasonicated to obtain a homogeneous solution, which was then cast into a Teflon mold and photo crosslinked by irradiation with UV light (λ = 365 nm) in a Teflon mold for 1 h at room temperature.

2.3. Nitrogen absorption

Nitrogen absorption isotherms were measured with an ASAP2010 adsorption analyzer (Micromeritics) at liquid-nitrogen temperature. Prior to the measurements, all samples were degassed at 250 °C for at least 3 h. The specific surface area was calculated from the adsorption data in the relative pressure interval from 0.04 to 0.2 using the Brunauer–Emmett–Teller (BET) method. Pore sizes distribution curves were calculated by the BJH method from the desorption branch. The total pore volume was estimated from the amount of nitrogen adsorbed at a relative pressure of 0.99.

2.4. Ionic conductivity

The ionic conductivity of the membrane was determined with an ac electrochemical impedance analyzer (PGSTAT 30); the experiments involved scanning the ac frequency from 100 kHz to 10 Hz, at a voltage–amplitude of 10 mV. The membrane (1 cm in diameter) was sandwiched between two smooth stainless tungsten–copper alloy disk electrodes in a cylindrical PTFE holder. The cell was placed in a thermally controlled chamber during the measurements. At a given temperature, the samples were equilibrated for at least 20 min before 90 repeated measurements were taken at 10 min intervals, or until no more changes in conductivity were observed. The ionic conductivity of the membrane was calculated from the observed sample resistance from the relationship:

$$\sigma = \frac{L}{RA} \tag{1}$$

where σ is the ionic conductivity (in S cm^{-1}), L is the distance between the electrodes used to measure the potential, R is the impedance of the membrane (in Ω) measured at the frequency that produced the minimum imaginary response, and A is the membrane section area (in cm^2).

The ionic conductivity of PIL-based membranes obtained at elevated temperatures can be used to estimate the activation energy (E_a) using the following Eq. (2)

$$\ln \quad \sigma = -\frac{E_a}{RT} \tag{2}$$

where σ is the ionic conductivity in S cm^{-1}, E_a is the activation energy in kJ mol^{-1}, R is the universal gas constant (8.314 J mol^{-1} K), and T is the absolute temperature in K.

2.5. Thermal analysis and leaching test

A DuPont Q100 thermo-gravimetric analyzer (TGA) was used to investigate the thermal stability of the membranes; the samples (~10 mg) were heated from ambient temperature to 850 °C under a nitrogen atmosphere at a heating rate of 10 °C min^{-1}. The leaching test was carried out by immersing membranes in Milli Q water with magnetic stir at room temperature. The membranes were removed from the water after 24 h and dried in a vacuum oven at 60 °C until a constant weight was achieved. Loss of ionic liquid from the membrane was determined gravimetrically. The ionic liquid loss after leaching test was calculated from the following equation:

$$\text{IL loss after leaching test}\,(\%) = \frac{W_I - W_L}{W_{IL}} \times 100\% \tag{3}$$

where W_I is the initial weight of membrane, and W_L is the weight of membrane after the leaching test. W_{IL} is the initial weight of IL in the membrane. The ionic conductivity loss was calculated according to the following equation:

$$\text{Ionic conductivity loss}\,(\%) = \frac{\sigma_I - \sigma_L}{\sigma_I} \times 100\% \tag{4}$$

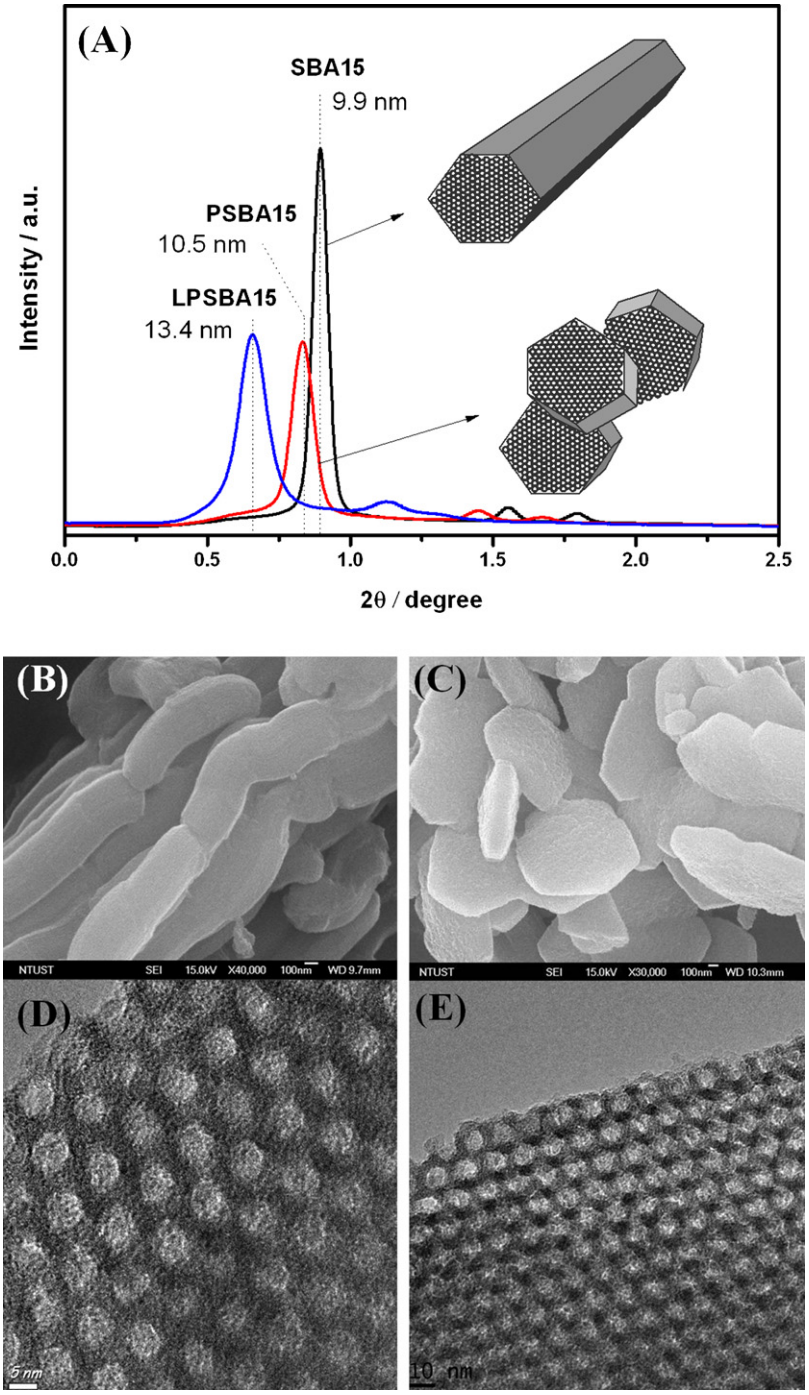

Fig. 1. (A) Small-angle XRD pattern using CuKα radiation source (λ = 1.5418 Å); SEM images of SBA15 (B) and P-SBA15 (C), TEM images of SBA15 (D) and P-SBA15 (E).

where σ_I is the ionic conductivity at 160 °C (in mS cm^{-1}), σ_L is the ionic conductivity at 160 °C (in mS cm^{-1}) after leaching test.

3. Results and discussion

In this study, two types of mesoporous silica materials (SBA15 and P-SBA15) were synthesized in accordance with methods given previously [21,26]. Fig. 1(A) shows that both SBA15 and P-SBA15 have three distinct diffraction peaks ($2\theta = 0.90°$, 1.56°, and 1.79° for SBA15; $2\theta = 0.84°$, 1.45°, and 1.67° for P-SBA15 indexed to the (1 0 0), (1 1 0), and (2 0 0) planes, respectively) of 2D hexagonal p6mm structure [27] and a narrow pore size distribution ($D = 9.9$ nm for SBA15; $D = 10.5$ for P-SBA15). The rod- or fiberlike morphology and long mesochannels of SBA15 are observable in the SEM photograph [Fig. 1(B)]. However, the morphology of P-SBA15 [Fig. 1(C)] is quite different from that of SBA15, in that it possesses hexagonal thin platelets and short mesochannels (the average thickness of the platelets is 150–350 nm). The TEM photographs [Fig. 1(D) and (E)] show that the mesoporous silica materials have well ordered pores arranged in a 2D hexagonal p6mm structure (the TEM image of LP-SBA15 is shown in Fig. S1).

Nitrogen absorption experiments for the BET (Brunauer–Emmett–Teller) analyses were conducted to measure the specific surface areas, porosities and average pore diameters of SBA15, P-SBA15 and LP-SBA15 as listed in Table 1 and Fig. S2. Both platelet and fiberlike SBA15 posses high surface

Table 1
Textural properties of S, SP, LSP composites.

Sample	Surface area ($m^2\ g^{-1}$)[a]	Pore volume ($cm^3\ g^{-1}$)[b]	Pore size (nm)[c]	Pore size (nm)[d]
SBA15	736.9	1.1	7.8	9.9
P-SBA15	774.8	1.511	9.5	10.5
LP-SBA15	571.9	1.774	17.4	13.4

[a] Calculated with the BET (Brunauer–Emmett–Teller) method.
[b] Accumulated pore volume with P/P_0 lower than 0.99.
[c] Obtained from N_2 absorption isotherm with the BJH (Barrett–Joyner–Halenda) method.
[d] Calculated from XRD.

areas ($700\ m^2\ g^{-1}$) and large pore volumes ($1\ m^3\ g^{-1}$). The pore diameters of platelet SBA15 are slightly larger than those of fiber-shaped SBA15. This is attributable to the P123 micelle having a hydrophobic core that expands as the hydrophilicity of the PEO chains decreases [21,28,29]. To aid discussion of the effects of the surface area and pore size on ionic conductivity, we also prepared platelet SBA15 (LP-SBA15) with a larger pore size (17.4 nm) and pore volume ($1.774\ m^3\ g^{-1}$) for comparison to P-SBA15.

The successful preparation of IL-based polymer electrolytes is critically dependent on the compatibility of the ILs and the polymeric matrix. Because the factors responsible for the miscibility of IL-based polymer systems are complex, it is still difficult to predict the compatibility of ILs with a given polymeric matrix. Poly(methyl methacrylate) (PMMA) is a commonly used polymer, due to its: ease of processing, low cost, and good mechanical properties. An ionic liquid has already been successfully used with PMMA for the preparation of a polymer electrolyte [11]. Free radical homo-polymerization of MMA and glycidyl methacrylate (GMA) has recently been conducted in ionic liquids using imidazolium salts [30]. Therefore, PMMA was chosen as the polymer matrix for the preparation of composite polyelectrolyte membranes in this work. The composite membranes were prepared via in situ photo crosslinking of a mixture of methyl acrylate (MMA) and divinyl benzene (DVB), together with various amounts of BMIm-TFSI and mesoporous silica materials in a Teflon mold. Fig. 2 shows photographs of the resulting PMMA/IL composite membranes containing various amounts of mesoporous silica fillers. These composite membranes are semitransparent, free-standing and flexible; additionally, they can be easily cut into any desired sizes and shapes.

Fig. 3 shows SEM micrographs of the fractured surfaces of the PMMA/IL/SBA15 and PMMA/IL/P-SBA15 composite membranes. It can be seen that the mesoporous silica fillers are homogeneously embedded in the composite membranes and that no obvious agglomeration of the inorganic fillers is apparent in either of the composite membranes with low silica loadings. When the silica loading was increased to 7 wt%, the PMMA/IL/P-SBA15 membrane retained its homogeneity; however, aggregated inorganic domains are clearly visible in the PMMA/IL/SBA15 membrane. This result indicates that the thin platelets and short mesochannels are more favorably dispersed in the composite membrane as compared with membranes that show the presence of rod- or fiber-shaped mesoporous silica fillers. The homogeneous distribution of the ionic liquid component in the composite membrane was observed from sulfur atom mapping (Fig. S3; SEM–EDS mapping). We surmise that the morphology of the mesoporous silica fillers and the related interface in the mixed PIL-based membrane are crucial factors that control the transport properties and the ionic conductivity of the PIL.

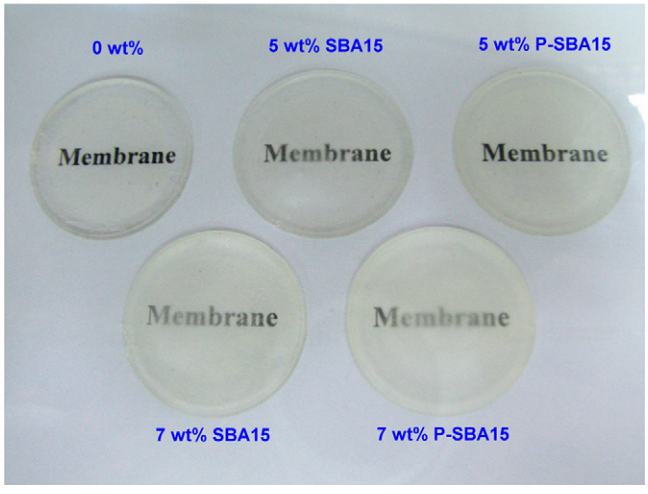

Fig. 2. Photographs of resulting PMMA/IL composites membrane containing various amounts of mesoporous silica fillers.

The ionic conductivities (σ) of PIL-based composite membranes containing 40 wt% of BMIm-TFSI, incorporated with various weight ratios of mesoporous silica fillers (SBA15 and P-SBA15) in anhydrous conditions were plotted as a function of temperature (40–160 °C) as shown in Fig. 4. The plain PMMA/IL membrane has an ionic conductivity that varies from $3.8 \times 10^{-3}\ S\ cm^{-1}$ at 40 °C to $2.3 \times 10^{-3}\ S\ cm^{-1}$ at 160 °C, a result that agrees well with previous reports [11]. The incorporation of silica materials into polymer membranes can have two competitive and opposing effects on the ionic conductivity [10,22,31–33]. The rigid and bulky mesoporous silica fillers tend to preclude close contact with surrounding polymer matrix chains and, thus, create a greater void volume around the mesoporous units of the composite [34]. Moreover, the well ordered pores of mesoporous silica favors the formation of PIL conducting continuous and interconnected channels in the composite membrane. A greater free volume and more interconnected channels, generally facilitates higher polymer electrolyte ionic conductivity. In contrast, the rigid and bulky structure of the mesoporous fillers tends to hinder chain movement and blocks the ion transport channels, which generally leads to lower ionic conductivities. Fig. 4 shows that the ionic conductivity of both composite membranes increased with an increase in the amount of the silica fillers; however, it abruptly decreased with the addition of excess fillers. This result indicates that a greater free volume and more interconnected channels are present at lower silica contents and that the further addition of silica has a blocking effect. As a comparison, the incorporation of the same weight ratio (5 wt%) of LP-SBA15 to P-SBA15, was found to raise the ionic conductivity of PMMA/IL/P-SBA15 ($9.4 \times 10^{-3}\ S\ cm^{-1}$) to about triple that of PMMA/IL/LP-SBA15 ($2.8 \times 10^{-3}\ S\ cm^{-1}$) at 160 °C. It can be clearly seen that higher surface area/volume ratios favor the formation of PIL conductive transfer channels and results in higher conductivity. However, it is worth noting that platelet SBA15 is more effective in improving the ionic conductivity of the PMMA/IL membrane compared to fiber-shaped SBA15. Membranes made with same content of mesoporous silica fillers (3 wt%), with various ratios of PIL, were also prepared and characterized. Fig. 5 clearly shows that with the incorporation of P-SBA15, a lower amount of the PIL ([MMA]/[PIL] = 3/1) can yield higher conductivity ($3.3\ mS\ cm^{-1}$),

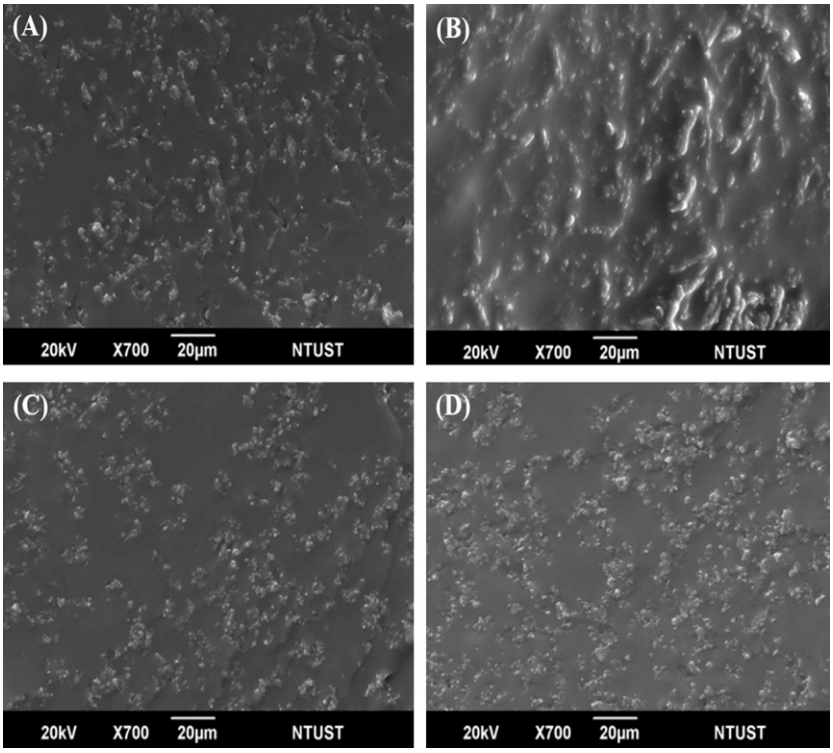

Fig. 3. SEM micrographs of the fractured surfaces of the PMMA/IL/SBA15 and PMMA/IL/PSBA15 composite membranes: (A) PMMA/IL/SBA15-3; (B) PMMA/IL/SBA15-7; (C) PMMA/IL/P-SBA15-3; (D) PMMA/IL/P-SBA15-7.

whereas a higher amount of the PIL ([MMA]/[PIL] = 2/3) is needed to reach a conductivity value close to those of the PMMA/IL/SBA15 (5.1 mS cm^{-1}) or the plain PMMA/IL (3.3 mS cm^{-1}) membranes. The mesoporous silica fillers in both the resulting pellet and the fiber-shaped structures have similar surface areas: therefore, we believe that the observed results may result from a higher number of interconnected nanopores and the shorter distance the ions have to travel – leading to more efficient ion transport in the shorter mesochannels of P-SBA15. In addition, SEM images show that the platelets and short mesochannels are more uniformly dispersed in the polymer membrane, which may improve the interconnectivity between the PIL domains for the transference of ions.

To clarify the effects of morphology and shape on the composite membranes, the activation energy (E_a) for ion transport, with respect to the two systems, was calculated. The fitting curve used to calculate the E_a values had temperature boundary conditions of 40 and 160 °C, the values determined by the application of the curve are presented in Table 2. Generally, the higher surface/volume ratio of the silica fillers led to a lower E_a due to the presence of additional internal conducting channels, and the possibility of enhanced ionic conduction at the mesoporous silica/electrolyte interface. It is not surprising that a small amount addition of P-SBA15 decreased the E_a value. The further addition of mesoporous silica fillers might block the ion transport channel resulting in a higher E_a value. However, the changing trend of E_a values of membranes with fiberlike SBA15 is quite different from platelet SBA15. In all cases, the membrane containing the SBA15 showed a higher E_a value (26.0–34.2 kJ mol^{-1}) as compared to a plain PMMA/IL membrane (E_a = 18.3 kJ mol^{-1}), this difference reflects the higher energy required for ion transfer through longer ion channels of SBA15. Moreover, the E_a values of all the IL-based composite membranes were higher than those of the Nafion 117 membrane saturated with water [35], showing that ion transfer needs more energy in the IL-based membranes. On the basis of the E_a values it can be concluded that ion transport within this type of IL-based membrane might have occurred by both mechanisms. These results are in good agreement with those found for other types of IL-based membranes [10].

Table 2
Energy of activation (E_a) for different PIL-based composite membranes.

Membrane	E_a (kJ mol^{-1})[a]
PMMA/IL	18.3
PMMA/IL/SBA15-1	26.0
PMMA/IL/SBA15-3	27.2
PMMA/IL/SBA15-5	30.4
PMMA/IL/SBA15-7	34.2
PMMA/IL/P-SBA15-1	17.5
PMMA/IL/P-SBA15-3	16.9
PMMA/IL/P-SBA15-5	26.8
PMMA/IL/P-SBA15-7	37.6

[a] Calculated from Eq. (2).

A criteria for developing high performance PIL-based membranes is that they should exhibit superior retention of the PIL in the membrane during long-term operation at high temperatures [17,36]. The PIL retention ability of membranes was confirmed by determining the percentage losses (%) of PIL from the membrane samples after immersion in distilled water, as shown in Fig. 6(a). It can be clearly seen that the incorporation of fiberlike SBA15 enhances the IL retention ability of the membrane. The enhancement of the IL-holding strength can be attributed to capillary forces within the mesoporous silica materials. However, the incorporation of a small amount of platelet SBA15 is not effective in enhancing the IL retention of the membrane, i.e., further additions of P-SBA15 are needed to create the shorter distances required for IL transfer through platelet SBA15 [21] leading to lower IL-holding strengths. Ionic conductivity measurements were carried out on leached samples to determine the drop in conductivity in comparison to non-leached membranes at 160 °C (see Table 3). The percentage losses (%) of ionic conductivities after leaching were

Table 3
Quantity of ionic liquid leached out and ion conductivity values of leached sample.

Sample	IL loss after leaching test (%)[a]	Conductivity at 160 °C (mS cm^{-1})		Conductivity loss (%)[b]
		Before leaching	After leaching	
PMMA/IL	41.8	2.3	0.9	60.9
PMMA/IL/SBA15-1	27.8	4.7	2.5	46.8
PMMA/IL/SBA15-3	22.4	3.1	1.9	38.7
PMMA/IL/SBA15-5	19.5	2.2	1.7	22.7
PMMA/IL/SBA15-7	17.3	1.6	1.3	18.8
PMMA/IL/P-SBA15-1	29.2	5.0	3.1	38.0
PMMA/IL/P-SBA15-3	24.5	7.2	5.3	26.4
PMMA/IL/P-SBA15-5	21.9	3.0	2.3	23.3
PMMA/IL/P-SBA15-7	19.7	2.3	1.8	21.7

[a] Calculated from Eq. (3).
[b] Calculated from Eq. (4).

also measured and is shown in Fig. 6(b). The ionic conductivity loss of the composite membrane was found to be strongly dependent on the weigh loss of PIL. Incorporation of SBA15 in the composite membrane can increase the IL retention ability, leading to a lower ionic conductivity loss. The highest ionic conductivity (5.3 mS cm^{-1}) was obtained by incorporating 5 wt% of P-SBA 15 in the membrane, this values is about six times that of a plain PMMA/IL membrane (0.9 mS cm^{-1}) at 160 °C after leaching. Based on the above observation, we tried to illustrate the possible ion and IL transport mechanisms for two systems (Scheme 1). Although, the capillary forces of the lengthy mesochannels impede the diffusion of the IL molecules, they also hinder ion transport through the membrane. In contrast, platelet and shorter mesochannels form continuous and shorter ion channels, which facilitate ion transport more effectively while retarding the release of IL from the membrane. Consequently, the morphology of mesoporous materials and its interrelationship with the interface in the composite membrane system is regarded as being crucial in controlling the diffusion properties of the PIL and the conductivity of the membrane.

Fig. 7 shows the thermal stability of the composite membranes examined with a thermogravimetric analyzer. All of the membranes lose less than 7% in weight up to 300 °C, confirming that both of PIL-based composite membranes have a high thermal stability, which is very suitable for high temperature application in PEMFCs. With the incorporation of P-SBA15 mesoporous silica, the value of $T_{10\%}$ (onset temperatures for weight losses of 10%) was considerably improved, reaching 355.8 °C for all of the composite membranes (PMMA/IL: $T_{10\%}$ = 336.4 °C). However, the value of T_{10} increased with the incorporation of small amounts of SBA15 and decreased with further additions of silica fillers. The results indicate that additional reinforcement of thermal properties was obtained via the incorporation of platelet SBA15 in the PIL-based membrane.

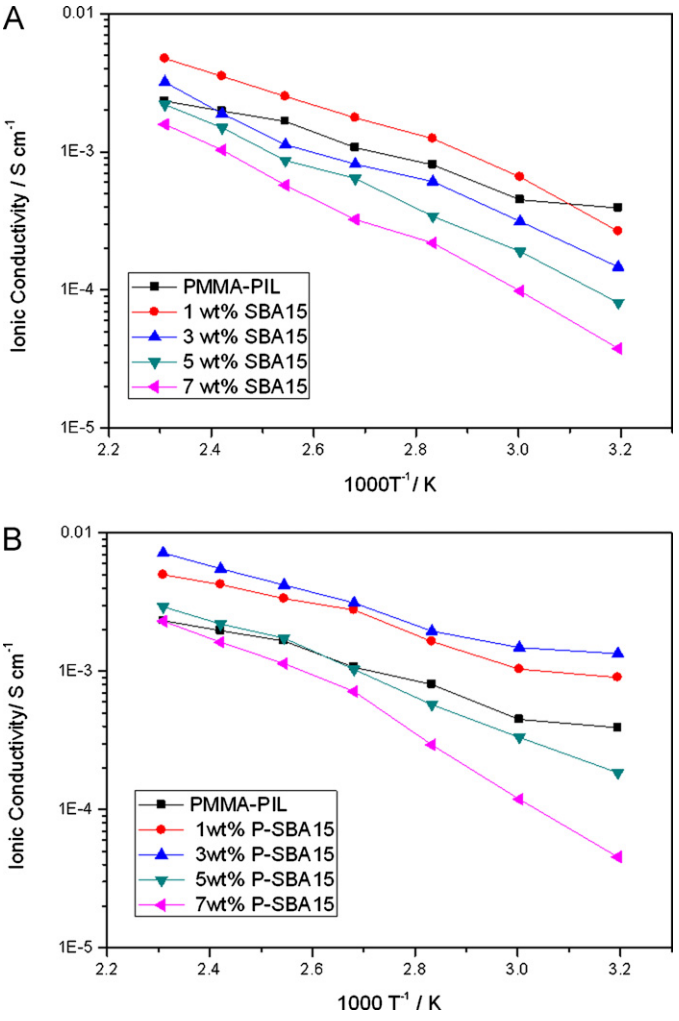

Fig. 4. The ionic conductivities (σ) of PIL-based composite membranes incorporated with various weight ratio of mesoporous silica fillers (SBA15 and P-SBA15) in anhydrous conditions plotted as a function of temperature (40–160 °C).

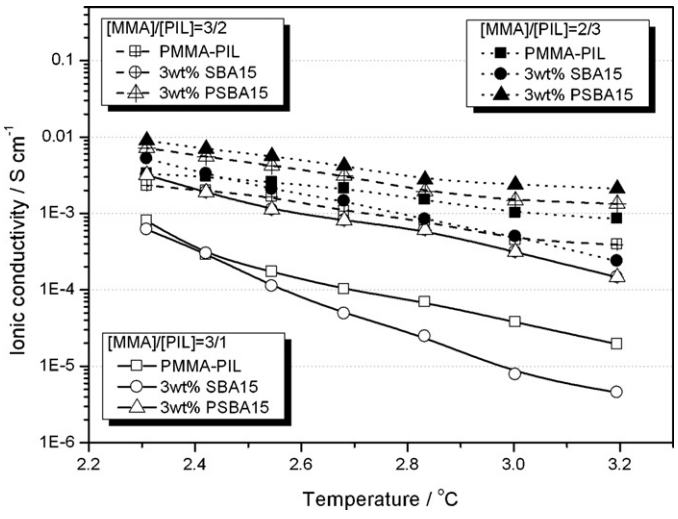

Fig. 5. The ionic conductivities of membrane incorporated with same content of mesoporous silica fillers (3 wt%) with various ratio of PIL.

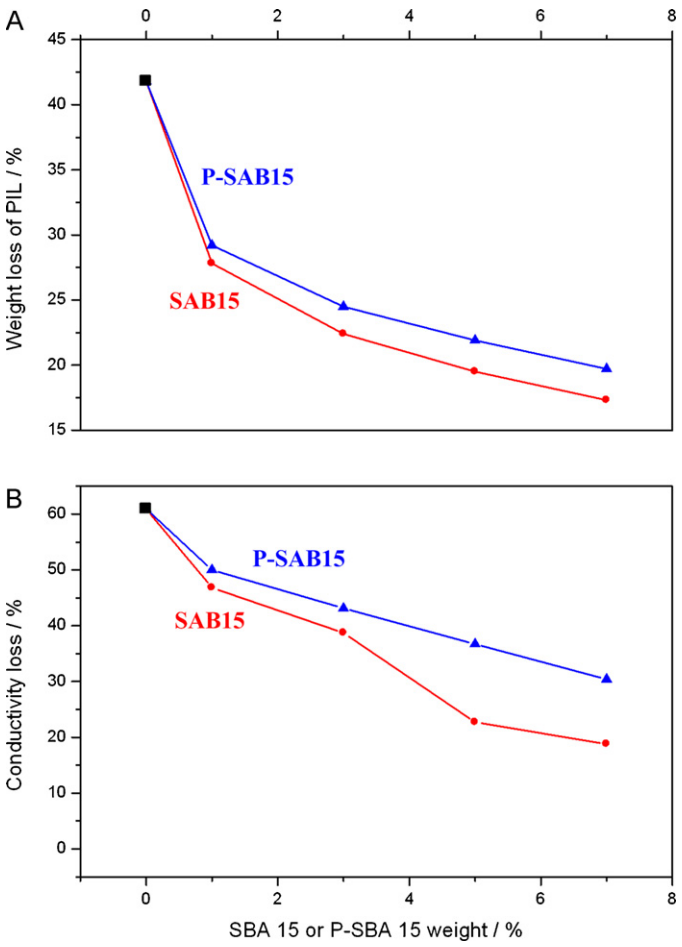

Fig. 6. (A) The percentage losses (%) of PIL from the membrane samples after immersion in distilled water. (B) The percentage losses (%) of ionic conductivities after leaching test.

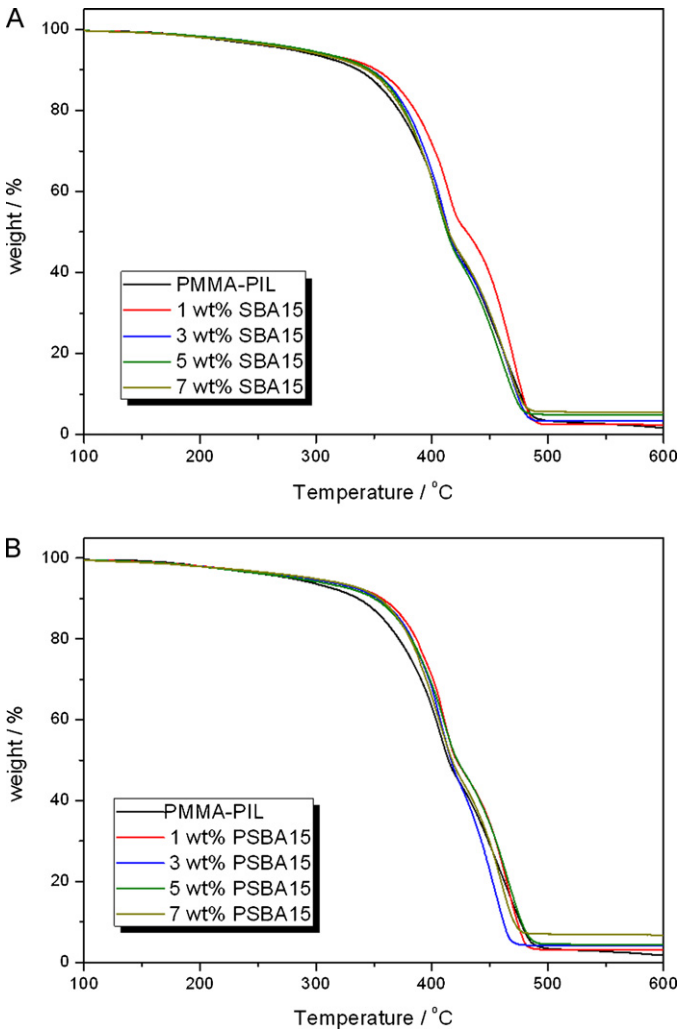

Fig. 7. The thermal stability of (A) PMMA/IL/SBA15 and (B) PMMA/IL/P-SBA15 composite membranes.

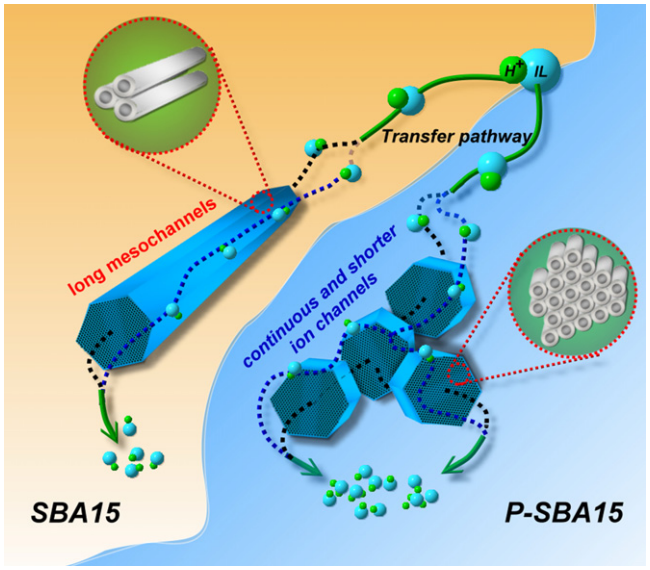

Scheme 1. Illustration of the ion and ionic liquid transport mechanisms in the membrane.

4. Conclusions

In summary, two types of SBA15 materials with platelet and fiberlike morphologies were synthesized and incorporated into IL-based membranes to form PMMA/IL/mesoporous silica composite membranes. The platelet shape and very short mesochannels (150–350 nm) increased their compatibility, resulting in better dispersion of these silica fillers within the polymer matrix and improved ion transport and thermal stability for PMMA/IL/P-SBA15 membranes relative to the PMMA/IL/SBA15 system. For the PMMA/IL/P-SBA15 membranes, a combination of the high surface/volume ratio and continuous and interconnected ion transport channels, are more effective in enhancing the conductivity. Compared with platelet SBA15, fiberlike SBA15, which has a higher IL-holding strength, is more effective in preventing the release of IL from the composite membranes. The highest ionic conductivity (5.3 mS cm^{-1}) was obtained by incorporating 5 wt% of P-SBA 15 in the membrane, this being about six times that of a plain PMMA/IL membrane (0.9 mS cm^{-1}) at 160 °C after leaching. We believe that the morphology of the mesoporous materials in the composite membrane is a crucial factor in controlling the diffusion properties of the PIL and the resulting conductivities of membranes.

Acknowledgements

We thank financial support from the National Science Council (under contract number NSC-99-2120-M-011-001), facilities from the National Taiwan University of Science and Technology, and the National Synchrotron Radiation Research Center (NSRRC) is gratefully acknowledged.

Appendix A. Supplementary data

Supplementary data associated with this article can be found, in the online version, at doi:10.1016/j.jpowsour.2011.02.066.

References

[1] M.S. Dresselhaus, I.L. Thomas, Nature 414 (2001) 332.
[2] K.D. Kreuer, S.J. Paddison, E. Spohr, M. Schuster, Chem. Rev. 104 (2004) 4637.
[3] M.A. Hickner, H. Ghassemi, Y.S. Kim, B.R. Einsla, J.E. McGrath, Chem. Rev. 104 (2004) 4587.
[4] C.Y. Wang, Chem. Rev. 104 (2004) 4727.
[5] Y.-S. Ye, Y.-J. Huang, C.-C. Cheng, F.-C. Chang, Chem. Commun. (2010).
[6] N.V. Plechkova, K.R. Seddon, Chem. Soc. Rev. 37 (2008) 123.
[7] O. Green, S. Grubjesic, S. Lee, M.A. Firestone, Polymer Rev. 49 (2009) 339.
[8] J.A. Asensio, E.M. Sanchez, P. Gomez-Romero, Chem. Soc. Rev. 39 (2010) 3210.
[9] J.A. Mader, B.C. Benicewicz, Macromolecules 43 (2010) 6706.
[10] B. Lin, et al., Chem. Mater. 22 (2010) 1807.
[11] M.A.B.H. Susan, T. Kaneko, A. Noda, M. Watanabe, J. Am. Chem. Soc. 127 (2005) 4976.
[12] F. Yan, et al., Chem. Mater. 21 (2009) 1480.
[13] M.K. Mistry, S. Subianto, N.R. Choudhury, N.K. Dutta, Langmuir 25 (2009) 9240.
[14] S.S. Sekhon, et al., Macromolecules 42 (2009) 2054.
[15] S.-Y. Lee, T. Yasuda, M. Watanabe, J. Power Sources 195 (2010) 5909.
[16] Y.S. Ye, et al., J. Mater. Chem. (2011).
[17] A. Fernicola, S. Panero, B. Scrosati, J. Power Sources 178 (2008) 591.
[18] E.-B. Cho, H. Kim, D. Kim, J. Phys. Chem. B 113 (2009) 9770.
[19] X. Ji, et al., Chem. Mater. 15 (2003) 3656.
[20] F. Li, A. Stein, Chem. Mater. 22 (2010) 3790.
[21] S.-Y. Chen, et al., Chem. Mater. 20 (2008) 3906.
[22] C.V. Subba Reddy, et al., J. Non-Cryst. Solids 353 (2007) 440.
[23] Y. Jin, et al., J. Power Sources 185 (2008) 664.
[24] F. Pereira, et al., Chem. Mater. 20 (2008) 1710.
[25] X. Wang, K.S.K. Lin, J.C.C. Chan, S. Cheng, Chem. Commun. (2004) 762.
[26] C. Yu, J. Fan, B. Tian, D. Zhao, Chem. Mater. 16 (2004) 889.
[27] D. Zhao, Q. Huo, J. Feng, B.F. Chmelka, G.D. Stucky, J. Am. Chem. Soc. 120 (1998) 6024.
[28] C. Li, et al., Chem. Mater. 19 (2006) 173.
[29] A. Kabalnov, U. Olsson, H. Wennerstroem, J. Phys. Chem. 99 (1995) 6220.
[30] J. Lu, F. Yan, J. Texter, Prog. Polym. Sci. 34 (2009) 431.
[31] M.J. Reddy, P.P. Chu, U.V.S. Rao, J. Power Sources 158 (2006) 614.
[32] J. Xi, et al., Solid State Ionics 176 (2005) 1249.
[33] Z. Wen, et al., J. Power Sources 90 (2000) 20.
[34] Y.-S. Ye, Y.-C. Yen, W.-Y. Chen, C.-C. Cheng, F.-C. Chang, J. Polym. Sci. Part A: Polym. Chem. 46 (2008) 6296.
[35] H. Pei, L. Hong, J.Y. Lee, J. Power Sources 160 (2006) 949.
[36] J.Y. Kim, et al., J. Membr. Sci. 283 (2006) 172.